

In-Vitro Assessment of the Functional Performance of the Decellularized Intact Porcine Aortic Root

Sotirios A. Korossis¹, Helen E. Wilcox¹, Kevin G. Watterson², John N. Kearney³, Eileen Ingham¹, John Fisher¹

¹Institute of Medical and Biological Engineering, University of Leeds, Leeds, ²Yorkshire Heart Center, Leeds General Infirmary, Leeds, ³National Blood Service Tissue Services R&D, Sheffield, UK

Background and aims of the study: Tissue-engineered heart valves offer the potential to deliver a heart valve replacement that will develop with the young patient. The present authors' approach is to use decellularized aortic heart valves reseeded in vitro or in vivo with the patient's own cells. It has been reported that treatment of porcine aortic valve leaflets with 0.1% (w/v) sodium dodecyl sulfate (SDS) in hypotonic buffer produced complete leaflet acellularity without affecting tissue strength. The present study aim was to investigate the effect of an additional treatment incorporating 1.25% (w/v) trypsin and 0.1% (w/v) SDS on the biomechanics and hydrodynamics of the aortic root. This treatment has been shown to produce decellularization of both the aorta and valve leaflets.

Methods: Fresh porcine aortic roots were treated to reduce the thickness of their aortic wall, and incubated in hypotonic buffer for 24 h. The leaflets were masked with agarose gel, and the aorta was treated with 1.25% (w/v) trypsin for 4 h at 37°C. The trypsin and agarose were removed and the roots incubated with 0.1% (w/v) SDS in hypotonic buffer for 24 h. Fresh and treated circumferential and axial aortic

specimens were subjected to uniaxial tensile testing, while intact porcine aortic roots were subjected to dilation and pulsatile flow testing.

Results: Decellularized aortic wall specimens demonstrated significantly decreased elastin phase slope and increased transition strain compared to the fresh control. However, the treatment did not impair tissue strength. Decellularized intact roots presented complete leaflet competence under systemic pressures, increased dilation and effective orifice areas, reduced pressure gradients, physiological leaflet kinematics and reduced leaflet deformation.

Conclusion: The excellent leaflet kinematics and hydrodynamic performance of the decellularized roots, coupled with the excellent biomechanical characteristics of their aortic wall, form a promising platform for the creation of an acellular valve scaffold with adequate mechanical strength and functionality to accommodate dynamic cell repopulation in vitro or in vivo. This approach can be used for both allogeneic and xenogeneic tissue matrices.

The Journal of Heart Valve Disease 2005;14:408-422

Tissue engineering offers the potential to create valve replacements from anatomically appropriate constructs containing autologous cells. A tissue-engineered valve replacement utilizing a sterile and functional scaffold, which would serve as a template for tissue development, could be a biocompatible structure that would adapt to the hemodynamics of

the body and function for the patient's lifetime. Moreover, the incorporation of viable cells derived from the host would enable anatomically appropriate and constant renewal of the complex extracellular valvular matrix that is progressively degraded during function (1).

Porcine aortic valves have been employed as scaffolds in the engineering of aortic valves because of their anatomical similarity to the human equivalent (1). In order to reduce the antigenicity of the xenograft material, several cell extraction techniques have been employed. The aim of these techniques is to create a non-toxic, non-immunogenic and non-calcific scaffold for subsequent reseeded with human autologous cells through either in-vitro cell seeding or in-vivo cell recruitment. These approaches can be used for both

Presented at the Second Biennial Meeting of the Society for Heart Valve Disease, 28th June-1st July 2003, Palais des Congrès, Paris, France

Address for correspondence:
Sotirios A. Korossis, Institute of Medical & Biological Engineering,
School of Mechanical Engineering, University of Leeds, Leeds LS2
9JT, UK
e-mail: s.korossis@leeds.ac.uk

allogeneic and xenogeneic scaffolds. Detergent-based cell extraction protocols (octyl-phenoxy-polyethoxy-ethanol (Triton X-100), sodium dodecyl sulfate (SDS), saponin), both with and without enzymatic digestion, have been shown to produce adequate cell and cellular antigen extraction (2-6). It is essential, however, that the treatment does not affect the (ultra)structural integrity of the extracellular matrix (ECM) proteins (glycosaminoglycans, elastin and collagen), as well as the biomechanical and hydrodynamic performance of the scaffold.

It has been reported that the treatment of porcine aortic roots with 0.1% (w/v) SDS produced complete leaflet decellularization, while retaining the (ultra)structural integrity of their ECM proteins (7). The treatment produced modest changes in extensibility of the leaflets without impairing their strength (8). Despite the success of this treatment in leaflet decellularization, it was not effective in decellularization of the aorta. Therefore, the SDS protocol was modified by including an enzymatic digestion step with 1.25% (w/v) trypsin. This dual process has been shown to produce decellularization of the aorta in addition to the leaflets (9). The present study focused on an investigation of the effect and implications of a novel decellularization treatment incorporating 1.25% (w/v) trypsin and 0.1% (w/v) SDS on the biomechanical integrity of the porcine aorta, and the hydrodynamic and dilation characteristics of the acellular intact porcine aortic root. This would determine the functional suitability of the acellular porcine aortic root as a scaffold for tissue-engineered valves. Moreover, the study would also determine the suitability of the particular decellularization protocol as a potential treatment for homografts.

Materials and methods

Tissue procurement and preparation

Twelve fresh porcine hearts were collected from a local abattoir within 4 h of slaughter. The animals were aged between 6 and 9 months. The aortic roots were excised from the hearts, trimmed of excess myocardium and connective tissue, and washed in phosphate-buffered saline (PBS). The coronary arteries were sutured, and the roots stored at 4°C in PBS, containing protease inhibitors (0.1% (w/v) ethylene diamine tetra-acetic acid (EDTA) and 10 KIU/ml aprotinin), until required (maximum 24 h after slaughter). The roots were then divided into two groups, each of six samples. The first group was left untreated and used as a fresh control; the second group was decellularized according to a previously published protocol (9).

Specifically, the aorta of the roots was thinned by

pulling off layers from the adventitia of about 2 mm thickness in total. This process is commonly used in the preparation of bioprostheses. The roots were placed in hypotonic buffer (50 mM Tris buffer, pH 8.0), containing protease inhibitors, incubated for 24 h at 4°C with agitation, and then washed (3_30 min) in PBS, containing 0.1% (w/v) EDTA, to remove the aprotinin. The valve leaflets were filled with 0.1% (w/v) agarose gel to protect and keep them hydrated during trypsin incubation, and the aorta was painted on both sides with 0.5% (w/v) agarose gel containing 1.25% (w/v) porcine trypsin. The roots were incubated for 4 h at 37°C in a humidified container, and then washed (3_30 min) with PBS containing protease inhibitors. This was followed by incubation in 0.1% (w/v) SDS in hypotonic buffer for 24 h at ambient temperature with agitation, and washing (3_30 min) with PBS containing 10 KIU/ml aprotinin. The roots were then incubated in nuclease solution containing 50 U/ml DNase, 10 U/ml RNase and 10 KIU/ml aprotinin for 4 h at 37°C with gentle agitation. Finally, they were washed (3_30 min) in PBS with protease inhibitors, and stored in PBS at 37°C for 2 days.

The fresh and decellularized roots were subjected to dilation and simulated pulsatile flow testing. Before testing, the roots were sized by measuring the external diameter at the commissures using Vernier calipers. The fresh roots were designated F1 to F6 in order of testing, whilst their size was between 23 and 25 mm (mean 24.0 ± 0.2 mm). The decellularized roots were designated D1 to D6 and were sized between 22 and 25 mm (following treatment) (mean 24.2 ± 0.4 mm). A one-way analysis of variance (ANOVA) showed that there was no significant difference between the size of the fresh and decellularized roots used ($p = 0.105$). Following function testing, one circumferential and one axial aortic wall strip were dissected from each root and subjected to uniaxial tensile testing.

Static leakage testing

Prior to the function testing, fresh and decellularized roots were subjected to static leakage testing in order to quantify the degree of their competence. The aorta of the root under investigation was mounted at the base of a pressure column, which was then filled with saline (0.9% (w/v) NaCl; Baxter) up to a height corresponding to a pressure of 100 mmHg. The time taken for the fluid to fall to the level corresponding to 80 mmHg was recorded. A particular root was considered to be competent if the pressure head had not fallen to 80 mmHg within a cut-off period of 15 min. If the root did not achieve this condition, it was discarded.

Root dilation testing

The purpose of the root dilation study was to quanti-

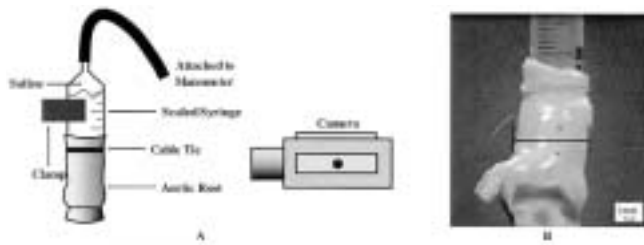


Figure 1: A) Side view schematic of the experimental setup used in the dilation tests. B) Method used to measure the circumferential dilation of the roots from the recorded images.

fy the effect imposed on the expansion characteristics of the aortic wall by the decellularization treatment. The roots were mounted in the dilation rig (Fig. 1A), and marked by two reference points placed axially, above the sinotubular junction (Fig. 1B). During dilation testing, the roots were pressurized from 0 to 120 mmHg in 20-mmHg intervals. At each increment, an image of the root, also showing the scaled syringe for subsequent calibration, was recorded using a video camera.

The acquired images of roots at each pressure interval were downloaded to a PC, where they were calibrated and analyzed using an image analysis software (Image Pro Plus™). The root dilation at a particular pressure was measured as the external root diameter half-way between the two reference points marked on the root (Fig. 1B). This ensured that dilation was measured at the same point regardless of axial elongation of the pressurized root. Root dilation at a particular pressure was expressed as the percentage change in root diameter from 0 mmHg. The dilation at each pressure increment was averaged over the number of roots in each group. The results were expressed as mean ± 95% confidence interval (95% C.I.), and plotted as a function of the applied pressure. The dilation results for the two test groups were compared using a one-way analysis of variance (ANOVA). The p-values from the ANOVA tables were used to determine statistical significance at the 0.05 cut-off level (95% confidence level).

Hydrodynamic function testing

The effect of treatment on the root hydrodynamics was assessed under simulated pulsatile flow. The flow simulator has been described previously (10), and was used to model the left side of the heart for testing valves in the aortic position. The blood substitute used in the test rig was physiological saline with a viscosity of 10^{-3} Pa·s. The test rig was operated under maximum compliance conditions, and all testing was conducted at 20°C. During testing, the diastolic/systolic pressure was set to 80/120 mmHg, whilst a 29-mm Björk-Shiley

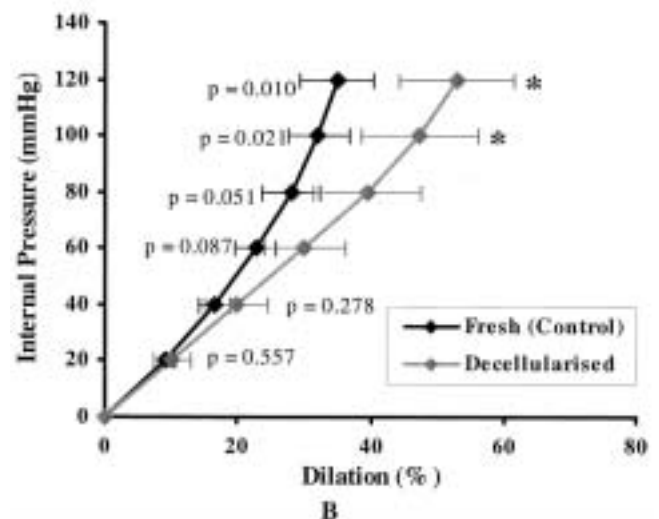
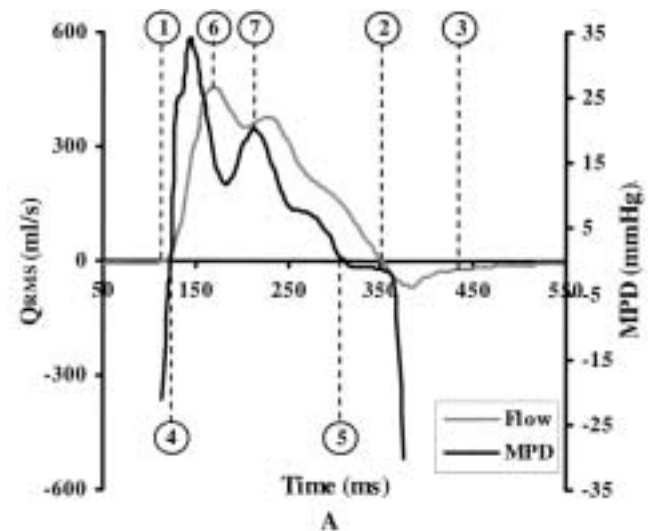


Figure 2: A) Sample flow and differential pressure signals showing the analysis intervals. B) Root dilation for fresh and decellularized roots as a function of internal pressure (mean ± 95% C. I., n = 6). *, significant difference, $p < 0.05$ (ANOVA).

tilting disc valve was used in the mitral position for all test runs.

The roots were mounted in the aortic position of the flow simulator using appropriately sized Delrin® spigots (10). During testing, the pressure difference across the roots was recorded using a differential pressure transducer (Gaeltec Model 3CT/Perspex). The flow through the roots was recorded using an electromagnetic flowmeter (Spectramed Blood Flow Meter, SP2202B). The roots were tested under five pulsatile flow conditions, corresponding to cardiac outputs of between 3.6 and 9.6 l/min (Table I). At each flow condition the roots were preconditioned for 50 cycles and tested five times to improve the repeatability of the results.

The hydrodynamic performance of the aortic roots was assessed by means of the mean pressure drop across the valve (MPD), the peak pressure drop (PPD) across the valve, the root mean square forward flow through the valve (QRMS), the peak forward flow through the valve (QPEAK), the valve effective orifice area (EOA), the reverse flow through the valve, and the valve energy losses. The calculation of these parameters was based on the recorded MPD and flow signals (Fig. 2A). The acquired pressure and flow signals for a particular cycle were defined by seven points. Point 1 marked the start of forward flow through the valve (start of systole); point 2 the end of forward flow (end of systole); and point 3 the end of closing valve regurgitation. The start of positive pressure was defined by point 4, and the end by point 5. Points 6 and 7 represented the instants of peak flow (peak systole) and pressure, respectively.

The MPD across each valve was assessed in the pressure-flow (PF) interval (4-2) as a function of the QRMS. MPD gives a measure of the degree of obstruction to blood flow, with lower pressure differences characterizing lower resistance to flow. The EOA index is another measure of the resistance to the flow through the valve under test, and this was also calculated for the PF interval. This index was normalized with respect to flow and was calculated from the pressure and flow measurements according to the experimental formula (11):

$$EOA = \frac{Q_{RMS}}{51.6 \times MPD} \quad (1)$$

Reverse flow through the valve was calculated during valve closing (dynamic regurgitation, interval 2-3) and when the valve was closed (static regurgitation, interval 3-1):

$$\begin{aligned} \text{Dynamic Regurgitation} &= \int_2^3 Q_{RMS}(t)dt \\ \text{Static Regurgitation} &= \int_3^1 Q_{RMS}(t)dt \end{aligned} \quad (2)$$

Energy losses due to fluid flow and pressure drop can be interpreted as valve efficiency factors and were calculated for the forward flow, closing and closed intervals according to:

$$\text{Energy Loss} = \int_{\hat{a}}^{\hat{a}} MPD(t)Q_{RMS}(t)dt \quad (3)$$

The results for each root were averaged over the five test runs conducted at each flow condition, and plotted as mean \pm 95% C.I. A one-way ANOVA was used to determine the statistical significance of the difference between the test groups at 95% C.I.

Leaflet kinematics and bending deformation analysis

Following hydrodynamic function testing, the valve leaflet kinematics of the fresh and decellularized roots was assessed by recording their leaflet motion under pulsatile flow. The assessment was conducted at flow condition B (72 cycles/min, stroke volume 70 ml), which gave a systolic duration of about 300 ms. For these experiments, a high-speed video camera system (Kodak Motion Corder Analyzer) was employed, which was positioned at a viewing port downstream of the root. The valves were illuminated externally by halogen spotlights and video frames were acquired at 500 frames per second for 2 s. The frame sequences were stored on video tape, and the frames corresponding to a complete cardiac cycle were stored in tagged image format on a PC for subsequent analysis. The acquired sequences allowed the opening, open and closing characteristics of the valve leaflets to be described. The assessed characteristics included opening, open and closing times, leaflet configurations, synchronization and abnormalities. Bending deformation along the free leaflet edge was also assessed throughout the cardiac cycle. Due to the experimental set-up and anatomical obstructions, the complete motion of only one whole leaflet could be recorded for the duration of the cardiac cycle. The coronary leaflets were larger than the non-coronary and, therefore, only the left coronary were used in order to analyze a longer

Table I: Flow conditions used in the hydrodynamic testing.

Flow condition	Cycle rate (bpm)	Stroke volume (ml)	Cardiac output (l/min)
A	60	60	3.60
B	72	70	5.04
C	80	70	5.60
D	100	80	8.00
E	120	80	9.60

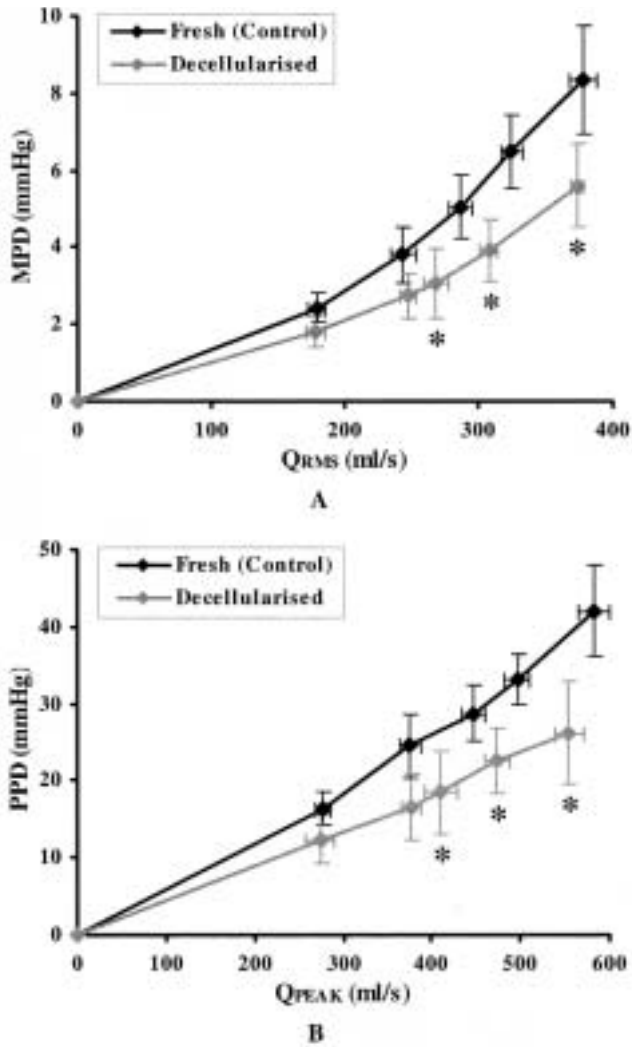


Figure 3: A) MPD against QRMS, and B) PPD against QPEAK for the two test groups (mean \pm 95% C. I., $n = 6$).
*, significant difference, $p < 0.05$ (ANOVA).

free edge and prevent any anatomical effects. Sequences of all three leaflets were also recorded to assess leaflet synchronization and configurations.

Leaflet bending deformation was assessed during three phases of the cardiac cycle. These included leaflet opening from fully closed (FC) to peak systole (PS), the interval that the leaflets were open from peak systole until starting to close at the end of systole (SC), and leaflet closing from the SC position until they were fully closed for the second time. Each phase was divided into equal-duration (± 2 ms) percentiles, and the video frames corresponding to 0, 25, 75 and 100% of the duration of each phase were analyzed to obtain the leaflet bending deformation. The leaflet reference state ($t = 0$) was defined at the instance where the leaflets were fully closed, immediately prior to the start of forward flow. The leaflet bending deformation at each

phase percentile was determined by the average curvature ($K_{i,avg}$) along the free edge of the leaflets (12). The curvature was defined quantitatively in the circumferential direction of the leaflets by the coordinates of the digitized traces of their free edge with respect to a reference origin. The digitized traces and the coordinates of the trace points for a particular leaflet and phase percentile were obtained by image analysis of the corresponding video frames using Image Pro Plus™. The calibration and subsequent analysis of the video frames, as well as the mathematical analysis of the calculation of $K_{i,avg}$ have been described previously (13). The $K_{i,avg}$ results for each leaflet and each percentile step during the opening, open and closing phases, were used to obtain the average bending radius ($R_{i,avg}$) as:

$$R_{i,avg} = \frac{1}{K_{i,avg}} \quad (4)$$

The calculation of bending strains assumes that there was no curvature of the leaflet in the neutral position. In the aortic valve, the physiological leaflet neutral geometry occurs with the aortic root dilated at systemic pressures (80-120 mmHg) and with no pressure difference across the valve. For both fresh and decellularized valves at the neutral position, the leaflets had an $R_{i,avg}$ of approximately 18 mm, which was quite large compared with the maximum values of minimum bending radii calculated for the fully open position (PS). It was, therefore, assumed that in the neutral position the leaflet was in a stress-free state, and thin shell theory was used to calculate the bending strain (ϵ_b) based on $R_{i,avg}$ and the thickness of the leaflet (t):

$$\epsilon_b = \frac{t}{2R_{i,avg}} \times 100 \quad (5)$$

The calculation of ϵ_b based on thin shell theory assumes that the leaflet thickness is uniform. The thickness of the left coronary leaflets of the fresh and decellularized roots was measured at 10 points along the leaflet free edge. The thickness was averaged over the number of readings for each leaflet ($n = 10$) and, subsequently, over the number of samples in each test group ($n = 6$). Although the thickness of the leaflets was not uniform along their free edge, a constant thickness was assumed, and thickness means of 0.19 mm for the fresh and 0.22 mm for the decellularized leaflets were used to simplify the calculation.

Biomechanical characterization

Following hydrodynamic function testing, tissue

strips were dissected from the aorta of the fresh and decellularized roots and subjected to low strain-rate uniaxial tensile loading to failure. The fresh tissue specimens were stripped off part of their adventitia, as with the case of the treated roots prior to decellularization. Circumferential and axial strips measuring 20×5 mm were dissected and mounted onto a purpose-built titanium holder (8). The holder was supported by a removable aluminum bracket that allowed alignment of the two holder parts, defined the gauge length of the specimens, and ensured that no load was imposed on the specimen until the start of the test. The gauge length of the specimens was defined by a 10 mm-wide central block separating the two holder parts and screwed onto the bracket. Before clamping, the thickness of the specimens was measured at six points

along their long axis using a Mitutoyo thickness gauge with a resolution of 0.01 mm, and their average thickness was recorded. During clamping, care was taken to mount the specimens under zero strain. Specifically, the wet specimen was floated onto the smooth clamp surface with minimum handling and secured at its completely relaxed state (8). Once the specimen was clamped onto the holder, the holder with the supporting bracket was secured to a Howden tensile machine and the bracket removed. Testing was conducted in physiological saline at 20°C (8).

Before loading to failure, the specimens were preconditioned by cycling loading using a double-ramp wave function until a repeatable load-elongation response could be observed. For all specimens tested, a preconditioning period of 50 cycles was sufficient to produce a steady-state response. Circumferential specimens were preconditioned between 0 and 110% and axial specimens between 0 and 90% at a rate of 10 mm/min. The strain limits were chosen to ensure that at least the transition phase of both specimen groups was reached. Following preconditioning, the specimens were loaded to failure using a positive ramp function at a rate of 10 mm/min. In order to obtain an accurate measure of the tissue gauge length, the tensile machine was set to produce a specimen preloading of 0.01 N before the operating program started to acquire any data. Therefore, zero extension was taken at the point where a 0.01 N load was detected. The final gauge length of the specimen was calculated as the initial gauge length (10 mm) plus the extension needed to produce the specified preloading. Failure was considered to occur when the first decrease in load was detected during extension. The mode of failure observed was middle section necking and rupture for 90% of the specimens, independent of the treatment, while the rest failed at the clamping point. During testing, load data from the load cell and extension data from the stroke of the tensile machine was acquired at a rate of 20 Hz. The engineering stress (σ) was calculated from the recorded load data as:

$$\sigma = \frac{F}{A_0} \quad (6)$$

where F is the acquired force in Newtons and A_0 the original cross-sectional area (CSA) of the undeformed specimen (in mm²). The CSA was calculated as $A_0 = w \times t$, where w is the width of the tissue strips (5 mm) and t their average thickness. The changes in thickness and width during preloading were considered negligible, and not taken into account. The engineering strain (ϵ) was calculated from the extension data according to the formula:

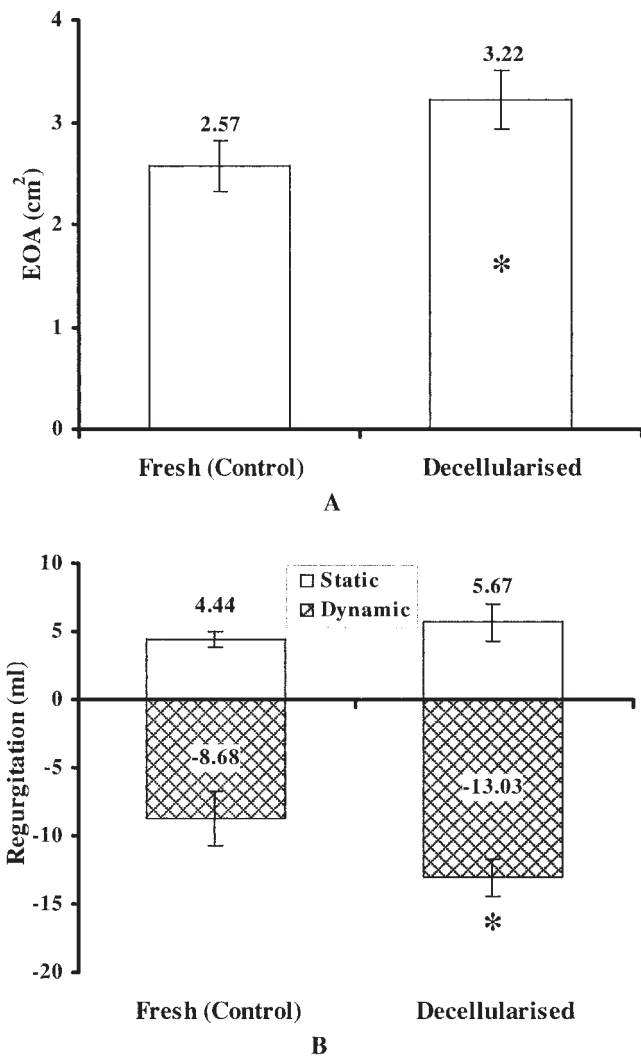


Figure 4: A) EOAs and B) regurgitation averaged over the five flow conditions, for fresh and decellularized roots (mean ± 95% C.I., n = 6). *, significant difference, $p < 0.05$ (ANOVA).

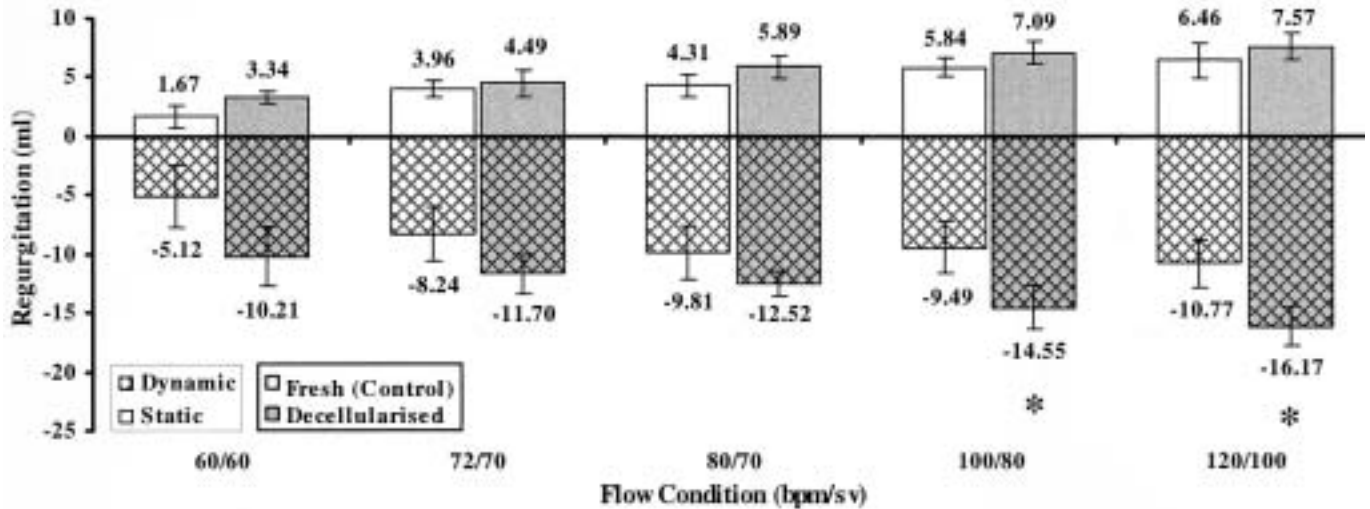


Figure 5: Regurgitation at each flow condition for fresh and decellularized roots (mean \pm 95% C. I., $n = 6$). *, significant difference, $p < 0.05$ (ANOVA).

$$\epsilon = \frac{\Delta l}{l_0} \times 100 \quad (7)$$

where Δl is the extension of the specimen and l_0 its final gauge length.

The calculated stress-strain curves obtained for the specimens of each group were averaged over the number of specimens in each group ($n = 6$) using a mathematical analysis software package (Origin v6.0, Microbal). The stress-strain behavior for each specimen was analyzed by means of six parameters. These have been described elsewhere (8), and included the elastin (El-E) and collagen (Col-E) phase slopes, transition stress (σ_{trans}) and strain (ϵ_{trans}), ultimate tensile strength (UTS) and failure strain (ϵ_{UTS}). The biomechanical parameters of the specimens in each test group were averaged, and compared by one-way ANOVA.

Results

Root dilation

For both test groups, the relationship between the average percentage dilation and applied pressure was to a good approximation linear up to the pressure of 60 mmHg, corresponding to the elastin phase of the aortic wall (Fig. 2B). Thereafter, the slope of the pressure-dilation curves demonstrated quasi-linear characteristics similar to the stress-strain behavior of aortic wall strips under uniaxial tension (see below). The decellularized roots demonstrated increased dilation compared to the fresh control for all applied pressures. The increase was not statistically significant up to 80 mmHg. However, in the physiological pressure range between 80 and 120 mmHg, dilation of the decellularized roots was significantly increased compared to that of the fresh roots ($p = 0.021$ and 0.010 , respectively).

Root hydrodynamic function

The average MPD was expressed as a function of the

Table II: p -values for Q_{RMS} , mean pressure drop (MPD), Q_{PEAK} and peak pressure drop (PPD) as determined by ANOVA between the fresh and decellularized groups at each flow condition ($n = 6$).

Flow condition	Q_{RMS}	MPD	Q_{PEAK}	PPD
60/60	0.172	0.104	0.274	0.233
72/70	0.185	0.065	0.201	0.060
80/70	0.061	0.033*	0.098	0.041*
100/80	0.052	0.009*	0.089	0.012*
120/80	0.129	0.013*	0.106	0.003*

*, significant difference ($p < 0.05$).

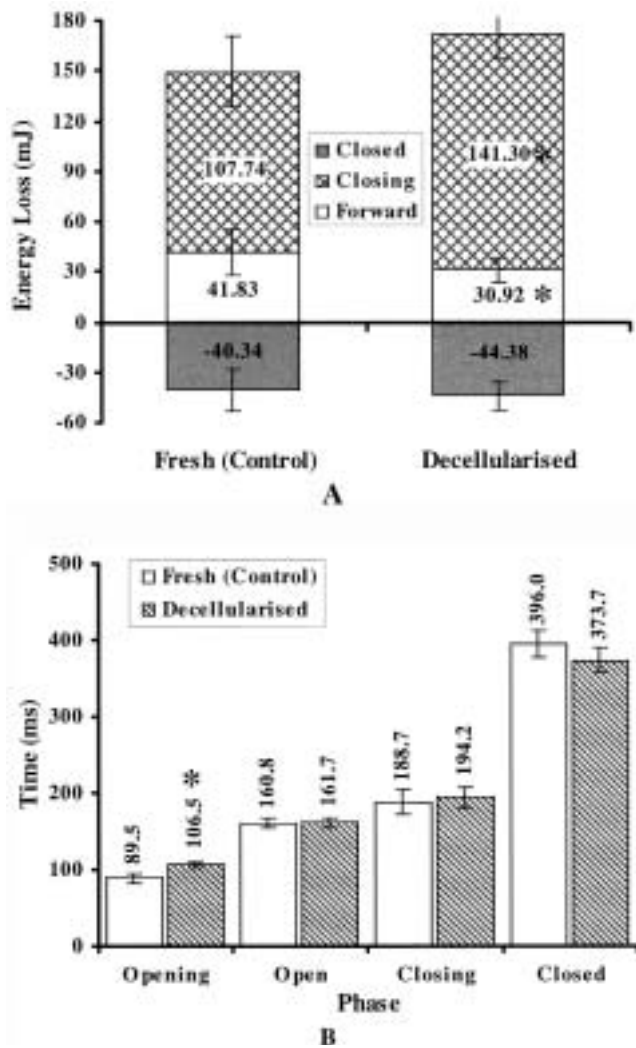


Figure 6: A) Energy losses averaged over the five flow conditions, and B) phase durations for fresh and decellularized valves at 72 bpm (mean \pm 95% C.I., $n = 6$). *, significant difference, $p < 0.05$ (ANOVA).

average QRMS (Fig. 3A). For all flow conditions, the difference in QRMS between the fresh and treated roots was not statistically significant (Table II). However, the difference in MPD was statistically significant at the three highest flow rates simulated ($p = 0.033, 0.009$ and 0.013). Since pulsatile flow testing of the roots was conducted under conditions of maximum compliance, the pressure oscillations usually observed under conditions of minimum compliance were eliminated. Therefore, the PPD could be used as an evaluation parameter. The average PPD as a function of the average QPEAK for the fresh and treated roots is illustrated in Figure 3B. The PPD was expressed as a function of QPEAK because of their approximate concurrence in the cardiac cycle (Fig. 2A, points 6 and 7). Similarly to the case of the MPD, the treated roots demonstrated significantly decreased PPD at the three highest simulated flows ($p = 0.041, 0.012$ and 0.003). There was no significant difference in the QPEAK between the two test groups (Table II).

The EOAs and regurgitation volumes of the two test groups were averaged over the five different flow conditions simulated and the sample population in each group (Fig. 4). The EOA of the decellularized group was significantly larger than that of the fresh ($p = 0.009$). For both groups, the measured dynamic regurgitation was negative, indicating back-flow or leakage through the valves. On the other hand, the static regurgitation of all roots was positive, indicating a forward flow and verifying competence of the roots since there was no back-flow through the fully closed valve. There was no statistical difference in the static regurgitation between the two groups ($p = 0.317$). However, the dynamic regurgitation of the treated roots was significantly increased ($p = 0.017$). For both groups, the regurgitation increased with increasing flow rates (Fig. 5), whereas a significant difference was observed in the dynamic regurgitation measured at the two highest flow conditions ($p = 0.011$ and 0.007).

With regards to the valve energy losses (Fig. 6A), the closed valve energy loss depicted the positive static regurgitation, whereas the closing energy loss was a result of the dynamic regurgitation. The forward flow

Table III: p -values for maximum bending strain as determined by ANOVA between the fresh and decellularized groups at each phase percentile ($n = 6$).

Phase percentage	Opening phase	Open phase	Closing phase
0	0.218	0.109	0.181
25	0.603	0.274	0.190
50	0.356	0.697	0.455
75	0.172	0.098	0.721
100	0.109	0.181	0.392

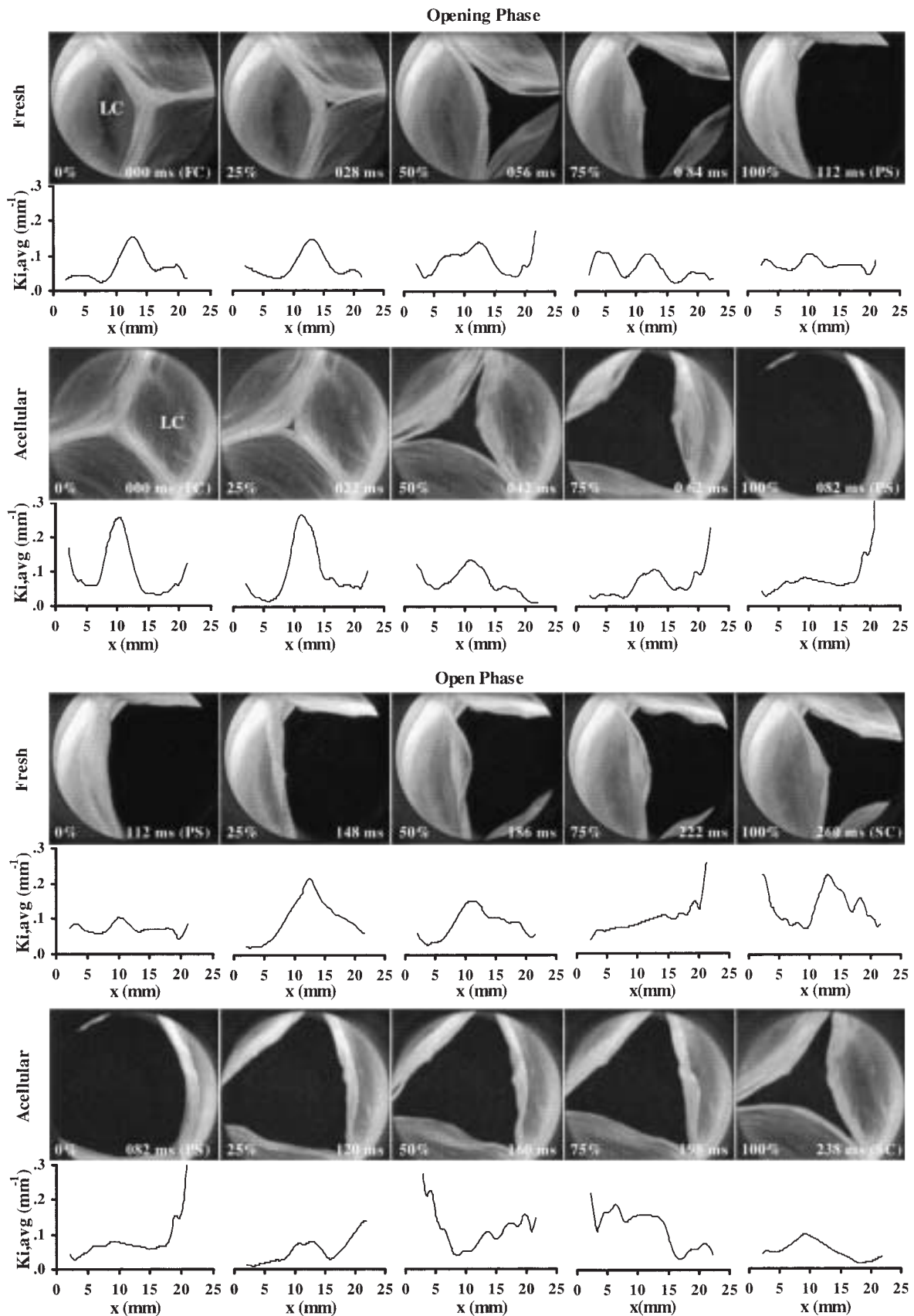


Figure 7: Sequence of the percentile video frames and the corresponding $K_{i,avg}$ profiles of the left coronary leaflet of the F1 (fresh) and D1 (acellular) roots during the valve opening and open phases.

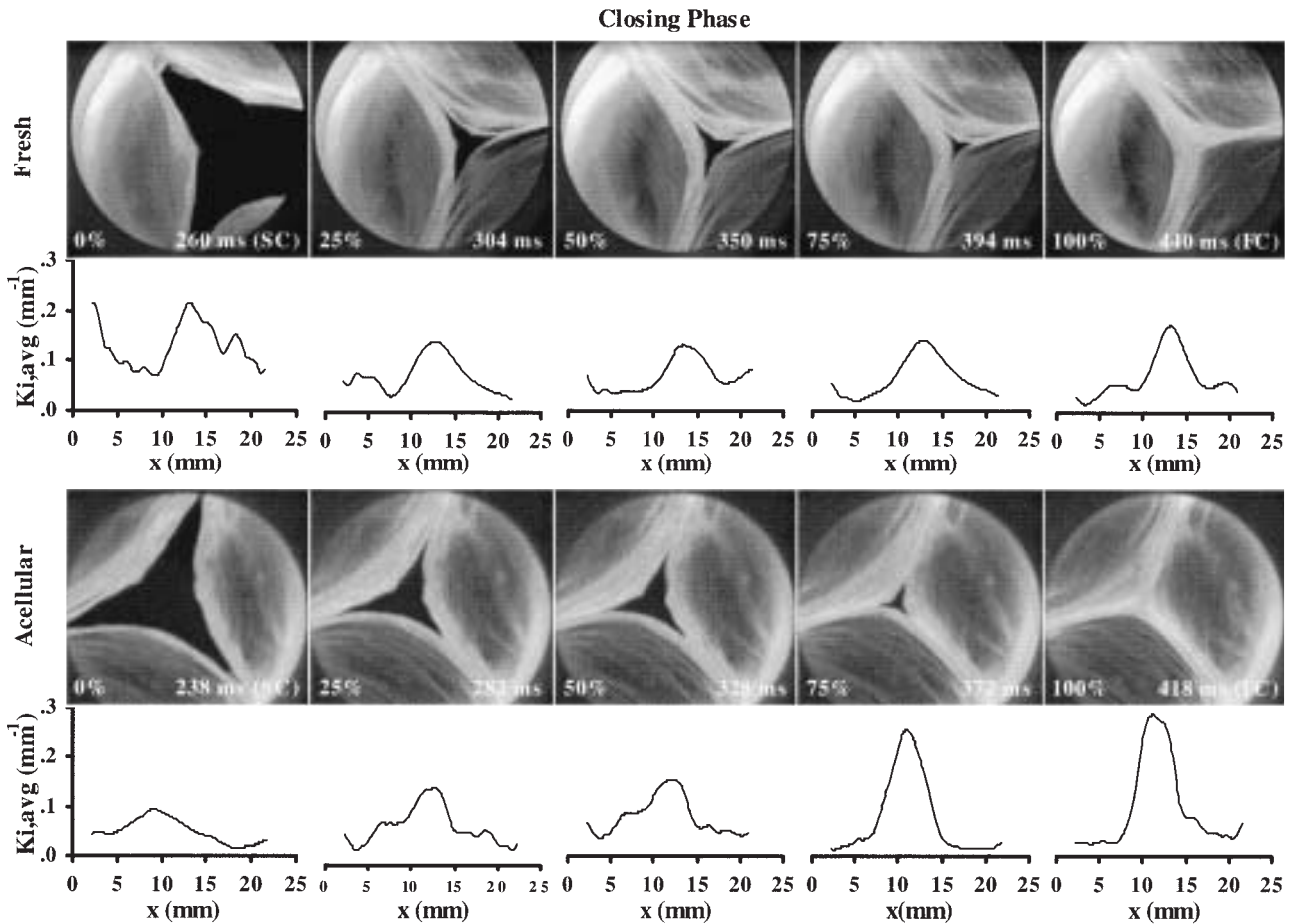


Figure 8: Sequence of the percentile video frames and the corresponding $K_{i,avg}$ profiles of the left coronary leaflet of the F1 (fresh) and D1 (acellular) roots during valve closing.

energy loss reflected the pressure-flow characteristics of the roots. The majority of the energy loss occurred during the closing phase, mainly due to the large closing regurgitation volumes. In contrast, forward flow energy losses were the smallest due to the low pressure drop across the roots. The decellularized roots demonstrated significantly decreased forward flow energy loss compared to the fresh control ($p = 0.010$). Significant difference was also observed in the energy

loss during valve closing, with the treated roots generating significantly increased loss ($p = 0.004$), mainly due to their significant increased regurgitation during this part of the cardiac cycle. The energy loss generated while the valves were closed was not statistically different between the two groups ($p = 0.422$). There was no significant difference in the total energy loss ($p = 0.098$).

Table IV: p -values for the biomechanical parameter as determined by ANOVA between the fresh and decellularized groups ($n = 6$).

Parameter	Col-E	otrans	etrans	oUTS	εUTS
EI-E					
Circumferential					
0.002*	0.059	0.061	0.002*	0.867	0.706
Axial					
0.056	0.108	0.432	0.994	0.414	0.307

*, significant difference ($p < 0.05$).

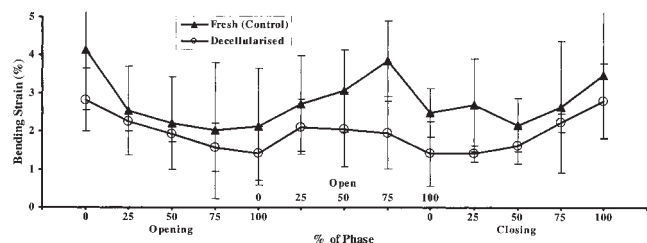
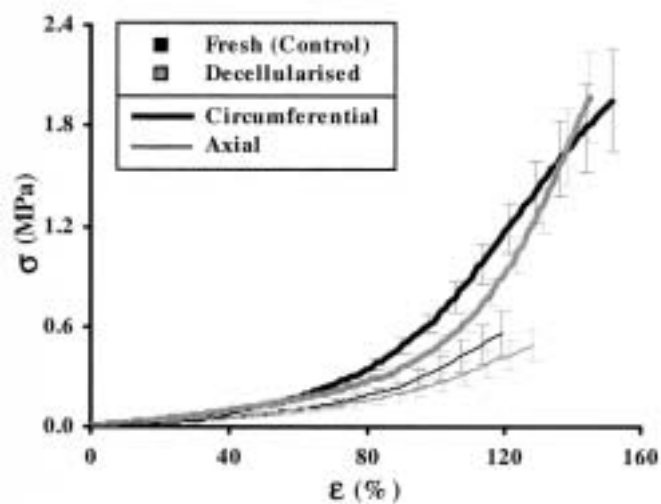


Figure 9: Maximum bending strain at each phase percentile for fresh and decellularized leaflets (mean \pm 95% C. I., $n = 6$).

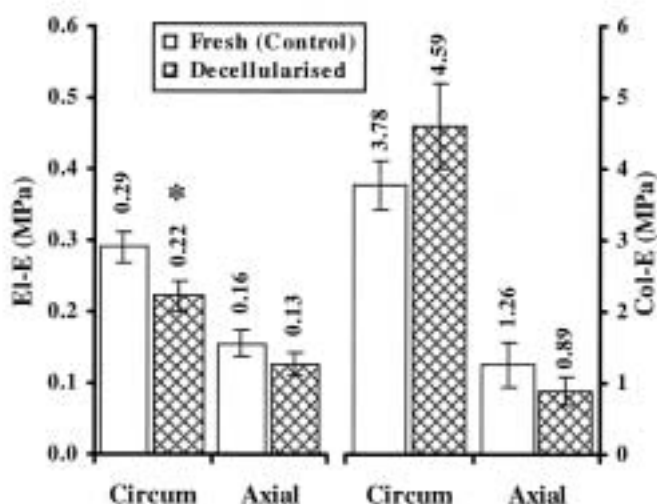
Leaflet kinematics and bending deformation

Preservation of compliance of the aortic root during treatment allowed systolic expansion of the leaflet commissures, which in turn generated a smooth opening and closing leaflet action in the decellularized roots. The opening phase duration of the decellularized valves was 106.5 ± 3.6 ms, which was significantly increased compared to that of 89.5 ± 6.3 ms for fresh valves ($p = 0.021$) (Fig. 6B). The difference in duration of the other phases was not statistically significant ($p = 0.727, 0.511$ and 0.070).

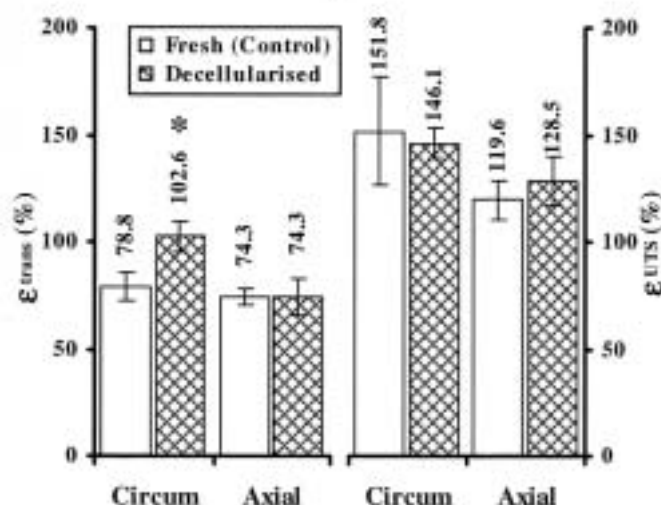
All decellularized valves demonstrated synchronous opening and closing (Figs. 7 and 8). During opening, the treated valves demonstrated the same stellate, triangular and circular leaflet configurations observed in



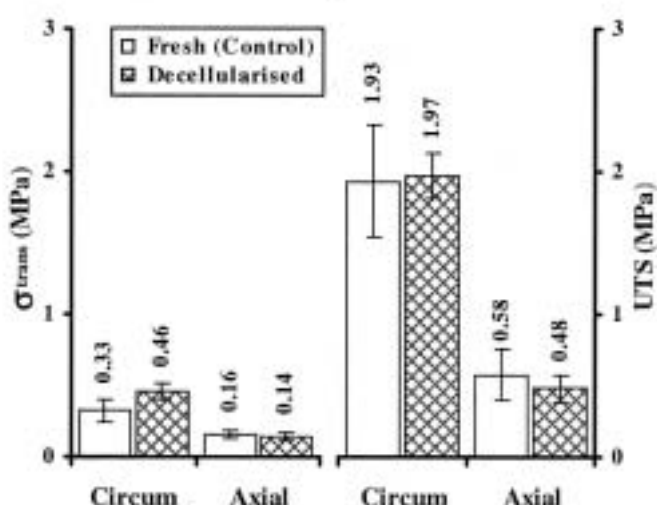
A



B



C



D

Figure 10: A) Stress-strain behavior; B) E_{l-E} and E_{col-E} ; C) ϵ_{trans} and ϵ_{UTS} ; and D) σ_{trans} and σ_{UTS} for fresh and decellularized circumferential and axial aortic wall specimens (mean \pm 95% C. I., $n = 6$). *, significant difference, $p < 0.05$ (ANOVA).

fresh valves. In the open phase, the decellularized valves showed the same mode of motion as fresh valves, with fluttering and slow closing before the final rapid closing phase. During diastole, all valves showed excellent closed leaflet configurations with no visible leakage orifices or coaptation flaws. Both fresh and decellularized valves demonstrated curvature spikes in the paracommissural area of their leaflets towards the end of the opening phase. For the rest of the cycle the largest curvatures were demonstrated in the middle portion of the leaflets.

The maximum bending strain (minimum $R_{i,avg}$, maximum curvature) experienced by the leaflets at each phase percentile was averaged for each test group; the strain variation throughout the three phases is illustrated in Figure 9. In all three phases, both fresh and decellularized groups demonstrated similar variation in the bending strain. During leaflet opening, the bending strain decreased due to the root dilation-assisted motion. In the closing phase, the strain started increasing again, until it reached the maximum of the fully closed position. The decellularized group demonstrated decreased levels of bending deformation compared to the fresh group, but there was no significant difference between them (Table III).

Biomechanics of the aortic wall

The stress-strain behavior of the aortic wall indicated that the anisotropy between its circumferential and axial directions was grossly maintained following decellularization (Fig. 10A). Closer study of the stress-strain behavior showed that the E1-E of the decellularized group in the circumferential direction was significantly reduced compared to the fresh control ($p = 0.002$) (Fig. 10B). This indicates that the treatment caused a reduction in tissue stiffness in the elastin phase, and this was in agreement with the dilation results obtained for the initial portion of the pressure/dilation curve (see Fig. 2B). A significant difference was also found in the tissue strain (Fig. 10C), with the decellularized group achieving increased levels of circumferential ϵ_{trans} ($p = 0.002$). Despite these differences between the test groups, the treatment did not compromise the strength of the tissue since no significant difference was observed in σ_{UTS} ($p = 0.867$ for the circumferential direction; $p = 0.414$ for the axial direction) (Fig. 10D). Similarly, there was no significant difference in any of the other circumferential and axial biomechanical parameters studied for the fresh and decellularized groups (Table IV).

Discussion

In the past, decellularization has been used as a means of developing non-immunogenic tissue scaffolds

for subsequent recellularization either in vivo or in vitro. Although many cell extraction techniques have been developed, few have been evaluated biomechanically, and none has undergone functional analysis (3,4,14,15). It has been reported previously that the treatment of porcine aortic leaflets with 0.1% (w/v) SDS in hypotonic buffer was sufficient to produce complete cell extraction without impairing their extracellular matrix integrity (7). That treatment produced a 25% increase in leaflet thickness (16% in the present study), modestly increased leaflet extensibility, as a result of tissue shrinkage, and preservation of the tissue strength. The results from that study also implied that the hypotonic buffer was responsible for the differences in the performance of the decellularized tissue compared to the fresh control (8). Porcine tissue was chosen not only as a potential xenogeneic matrix, but also as a model for allogeneic valves which are commonly used clinically, in their non-decellularized form.

SDS is an ionic ligand which binds to proteins via its hydrophobic domain, leaving its hydrophilic region exposed and thus generating an increased negative charge. Several studies have suggested that this increase in tissue charge leads to a near three-fold increase in tissue thickness due to increased water binding, and a significant fall in the shrinkage temperature of collagen (5,14,16). In these reported studies, however, the decellularization protocols employed 1% (w/v) SDS, and the fact that the treatments generated significant swelling may be true considering the high concentrations of detergent. On the other hand, treatment with 0.1% (w/v) SDS in hypotonic buffer produced complete cell extraction without compromising the ECM proteins or producing additional swelling to that generated by the buffer.

Despite the success of the treatment in decellularizing valvular leaflets, it caused minimal decellularization of the aortic wall. On this basis, the treatment was modified by the addition of 1.25% (w/v) trypsin. The dual enzymatic-detergent protocol, coupled with thinning of the aortic wall, produced complete cell extraction from the both the leaflets and aortic wall (9). In addition, the treatment did not affect most of the biomechanical parameters of the aorta, including its UTS. However, the decellularized aortic wall demonstrated a significant reduction in the stiffness of its elastin phase along the circumferential direction. This observation was also apparent in the dilation behavior of the decellularized roots, though in this case the difference compared to the fresh control was not significant. Generally, the decellularized roots demonstrated increased dilation compared to the fresh for all applied pressures. In the physiological pressure range the increase in dilation became significant, and this may have implications in vivo. Nevertheless, if the decellu-

larized valve is used as a free-sewn graft, the host aorta will restrict the increased dilation of the graft.

Hydrodynamic function testing has demonstrated significant differences between the behavior of fresh and decellularized roots. The decellularized valves demonstrated favorable pressure-flow characteristics, with lower MPD and PPD across them. Although no significant differences were observed between the two test groups at the lower flow rates, the difference in both MPD and PPD was significant at the three higher flow rates. The favorable pressure-flow characteristics of the decellularized group were also reflected in its significantly increased EOA. This behavior can be mainly attributed to the mechanical properties of the decellularized leaflets and aorta. It has been reported previously that 0.1% (w/v) SDS-treated leaflet specimens, when subjected to uniaxial tension, showed a significant reduction in the elastin phase modulus in both the circumferential (53%) and radial (45%) directions compared to the fresh control (8). Consequently, this reduction in stiffness of the leaflets increased their compliance. At peak systole, the increased compliance of the leaflets would have caused them to distend more in both directions, increasing the actual valve orifice and, consequently, decreasing the pressure drop. Moreover, the increased dilation of the decellularized group in the physiological pressure range, contributed further to its favorable performance.

The increased leaflet compliance of the decellularized roots also impacted on their significantly increased dynamic regurgitation. Since the leaflets distended more during opening, their area was increased, sweeping more fluid back on closing than did the fresh leaflets. The positive static regurgitation measured verified that both groups were competent, since there was no backward flow through the fully closed valves. This was confirmed by video analysis, which showed no visible orifices on the fully closed valves. The positive static regurgitation and the large closing regurgitation can be attributed to the effect of the dynamic and highly compliant aortic root on the flow. During ventricular systole, and as the aortic pressure rose from 80 to 120 mmHg, the aortic root dilated and reached a maximum dilation at peak systole. This generated an axial compression in the compliant root, which in turn caused a slight movement of the leaflet commissures towards the center of the root, in the direction of flow. During valve closing and as the root dilation relaxed, the valve moved backwards, resuming its original closed position at 80 mmHg. The flow associated with this backward movement would have been measured by the flowmeter as added closing regurgitation. Moreover, the decrease in root dilation forced fluid away from the valve. Since the valves were fully competent, the fluid could only move forward, and as the

flowmeter was placed downstream of the valve this was interpreted as positive forward flow and registered as static regurgitation.

For increasing flow rates the average static regurgitation for both groups also increased. However, for increasing flow rates the time for which the valve remained closed was decreased. This means that, in theory, the static regurgitation should also decrease. The fact that it actually increased can be attributed to flow oscillations induced by the highly compliant roots. The frequency of these oscillations increased with increasing flow rates, and could also explain the increase in dynamic regurgitation with increasing rates. Regurgitation volumes should be regarded with caution when used in the evaluation of hydrodynamic performance. This is especially the case for dynamic regurgitation, since the rapid rise in ventricular pressure at the start of systole (see Fig. 2A) may have forced more fluid back through the valves during closing than would normally occur clinically. With regards to energy losses, the forward flow energy loss was primarily due to the conversion of potential energy to kinetic energy as the flow was accelerated through the valve. For both groups, the forward flow energy loss was the smallest due to the small pressure difference at this phase. Both closing and closed energy losses are dependent on root compliance as they are representative of the regurgitant volumes. The decellularized roots demonstrated a significantly decreased forward flow energy loss due to the smaller MPD, and a significantly increased closing energy loss due to the higher dynamic regurgitation. There were no significant differences in the closed or total energy losses.

During opening, the decellularized valves demonstrated the same stellate, triangular and circular leaflet configurations observed in the native valve. At peak systole, they demonstrated a circular leaflet configuration, allowing for maximum flow, whereas during diastole they showed no visible orifices or coaptation flaws. They also demonstrated synchronous opening and closing leaflet motion, and decreased leaflet fluttering during the open phase. Preservation of compliance of the decellularized leaflets and aortic wall generated smooth valve opening and closing. However, the increased compliance of the leaflets caused them to take a longer time to respond to the dilation of the aorta generated by the pressure increase during systole and, therefore, the opening phase duration of the decellularized group was significantly increased compared to the fresh. Despite the increased compliance of the decellularized leaflets, they did not show any excessive sagging under the transmural pressure during diastole. This was another consequence of the increased dilation of the acellular roots, which largely compensated for the sagging of their highly compliant leaflets.

As a result of the root dilation-assisted motion, both fresh and decellularized leaflets demonstrated low paracommissural deformation. At peak systole, most of the leaflets analyzed had a small, almost uniform curvature. Nevertheless, some leaflets did present a paracommissural curvature spike when fully opened. These spikes were equally present in both groups, and there was no trend to indicate that they were more associated with the decellularized leaflets. Indeed, throughout the cardiac cycle both groups showed similar variation in maximum bending strain. However, for all phase percentiles the values obtained for the decellularized leaflets were smaller (though not significantly so) than those obtained for the fresh. The reduced bending deformation of the decellularized leaflets indicates that their length with respect to their intercommissural spacing was decreased compared to the fresh valves due to the increased dilation of the decellularized roots. This increased the bending radius of the leaflets, decreasing their bending deformation during systole.

In conclusion, the thorough in-vitro assessment of the effect of this novel decellularization treatment on the function of porcine aortic valves has shown that the differences previously found in the biomechanical properties with fresh valves have not translated into inferior functional performance and characteristics. It is therefore unlikely that these changes will significantly compromise valve function or accelerate degenerative failure in vivo. These results suggest that the decellularized valves have the mechanical and functional integrity to resist physiological flow conditions for at least short-term implantation. However, further studies on the durability of these valve scaffolds in an animal model should be conducted in order fully to elucidate and appreciate the effect of the treatment.

Acknowledgements

These studies were funded by the Yorkshire Children's Heart Surgery Fund (Leeds General Infirmary, Leeds, United Kingdom), and the Engineering and Physical Sciences Research Council Portfolio Award.

References

1. Eyre D R. Collagen molecular diversity in the body's protein scaffold. *Science* 1980;207:1315-1322
2. Bader A, Schilling T, Teebken OE, et al. Tissue engineering of heart valves: Human endothelial cell seeding of detergent acellularized porcine valves. *Eur J Cardiothorac Surg* 1998;14:279-284
3. Wilson GJ, Courtman DW, Klement P, Lee JM, Yeager H. Acellular matrix: A biomaterials approach for coronary-artery bypass and heart-valve replace-

- ment. *Ann Thorac Surg* 1995;60(Suppl.):S353-S358
4. Courtman DW, Pereira CA, Omar S, et al. Biomechanical and ultrastructural comparison of cryopreservation and a novel cellular extraction of porcine aortic valve leaflets. *J Biomed Mater Res* 1995;29:1507-1516
5. Courtman DW, Pereira CA, Kashef V, et al. Development of a pericardial acellular matrix biomaterial-biochemical and mechanical effects of cell extraction. *J Biomed Mater Res* 1994;28:655-666
6. Schmit CE, Baier JM. Acellular vascular tissues: Natural biomaterials for tissue repair and tissue engineering. *Biomaterials* 2000;21:2215-2231
7. Booth C, Korossis SA, Wilcox H, et al. Tissue engineering of cardiac valve prostheses I: Development and histological characterization of an acellular porcine scaffold. *J Heart Valve Dis* 2002;11:457-462
8. Korossis SA, Booth C, Wilcox H, et al. Tissue engineering of cardiac valve prostheses II: Biomechanical characterization of decellularized porcine aortic heart valves. *J Heart Valve Dis* 2002;11:463-471
9. Wilcox H, Korossis SA, Booth C, et al. Tissue engineering a living heart valve: Biocompatibility and recellularization potential of an acellular porcine heart valve matrix. *J Heart Valve Dis* 2005;14:212-217
10. Revanna P, Fisher J, Watterson KG. The influence of free hand suturing technique and zero pressure fixation on the hydrodynamic function of aortic root and aortic valve leaflets. *Eur J Cardiothorac Surg* 1997;11:280-286
11. Gabbay S, McQueen DM, Yellin EL, Becker RM, Frater RW. In vitro hydrodynamic comparison of mitral valve prostheses at high flow rates. *J Thorac Cardiovasc Surg* 1978;76:771-788
12. Corden JM, David T, Fisher J. Determination of the curvatures and bending strains in open trileaflet heart valves. *Proc Inst Mech Eng* 1995;209(H2):121-128
13. Korossis SA. Biomechanics and hydrodynamics of decellularised porcine aortic valves for tissue engineering. PhD Thesis, University of Leeds, 2002
14. Bodnar E, Olsen EGJ, Florio R, Dobrin J. Damage of porcine aortic valve tissue by the surfactant sodium-dodecyl-sulfate. *Thorac Cardiovasc Surg* 1986;34:82-85
15. Hirsch D, Drader J, Thomas TJ, Schoen FJ, Levy JT, Levy RJ. Inhibition of calcification of glutaraldehyde pre-treated porcine aortic valve cusps with sodium-dodecyl-sulfate: Pre-incubation and controlled released studies. *J Biomed Mater Res* 1993;27:1477-1484
16. Samouillan V, Dandurand-Lods J, Lamure A, et al. Thermal analysis characterization of aortic tissues for cardiac valve bioprosthesis. *J Biomed Mater Res* 1999;46:531-538

Meeting discussion

DR. SIMON P. HOERSTRUP (Switzerland): The ultimate fate of the decellularization approach will be an absence of cells, no immunology, and an absence of infection. You showed hematoxylin and eosin staining as proof of absence of cells, but that is not very strong evidence. Do you use other methods to show that there are no cell remnants left in the tissue?

DR. SOTIRIOS A. KOROSSIS (Leeds, UK): Unfortunately, we have not characterized the tissue in any other way to show if there are any cell remnants.

DR. JOHN FISHER (Leeds, UK): Could I make a comment? We have performed separate animal studies to examine the biocompatibility and immunological response of the tissue.

DR. CRYSTAL CUNANAN (USA): Two questions please. First - when you use SDS in the decellularization process, do you know if there is any residual SDS left in the tissue?

DR. KOROSSIS: No. We have performed cytotoxicity studies, and could not see any evidence of SDS present.

DR. CUNANAN: I would suggest that you macerate the valve with some saline - if you see soap bubbles, then you have residuals. SDS binds, but doesn't necessarily flush out. My second question is that because you are using SDS, and based also on some of your histology slides, you may be affecting the glycosaminoglycans in the tissue. That will affect the water in the tissue, and the swelling pressure, and the biomechanics. In your kinematic pictures, the decellularized valve seemed to be more translucent than the fresh valve.

DR. KOROSSIS: Yes, we noticed that it seemed to be more translucent.

DR. CUNANAN: So you may want to examine the water content as well as the glycosaminoglycans - to see if you have influenced it?

PROF. SIR MAGDI YACOUB (London, UK): How fresh were your fresh valves. Specifically, were the cells living - and do you think it matters?

DR. KOROSSIS: The valves were tested within 24 h of slaughter. I don't think the cells were living, but I don't know if that would produce any different results.

DR. MANO J. THUBRIKAR (Carolina, USA): The biomechanic studies seemed rather straightforward. Did you perform any experiments with the intact aortic root in terms of circumferential and longitudinal extensions comparing the non-decellularized and decellularized? Did you perform extension experiments with the intact aorta itself so that you could see the diameter and length changes and compare them in the two situations? These were uniaxial studies - they were not pressurized aorta studies. Correct?

DR. KOROSSIS: I did show some dilational results, in which the intact aortic root was pressurized.

DR. THUBRIKAR: But did you have the data for the longitudinal extensions? Can you comment on that?

DR. KOROSSIS: No, I only measured the circumferential dilation.

DR. THUBRIKAR: And was the longitudinal length fixed?

DR. KOROSSIS: No, the valve was just attached from the aorta. The other end was free to expand.

DR. THUBRIKAR: So it was free to lengthen, and not just to expand the diameter?

DR. KOROSSIS: Yes.

DR. THUBRIKAR: Do you not have the data for how the lengthening compared?

DR. KOROSSIS: Not at this point.

DR. THUBRIKAR: Thank you.

DR. EILEEN INGHAM (Leeds, UK): A comment about an earlier question. From a biological viewpoint, we looked at the glycosaminoglycan and collagen contents of these decellularized valves, and found there to be no effect. We also performed extract cytotoxicity tests to seek residuals of SDS. The extracts had no effect on cell viability - in fact, the concentration of SDS used in this procedure was much less than was used in previous studies.